Appl Phys B
DOI 10.1007/s00340-010-4154-z

Applied Physics B
Lasers and Optics

Frequency stabilization of multiple lasers and Rydberg atom spectroscopy

P. Oxley · P. Collins

Received: 19 February 2010 / Revised version: 20 May 2010

Abstract In this paper we report details of the apparatus and experimental techniques used to excite Rydberg states of ^{7}Li using multiple diode lasers. Special attention is paid to frequency stabilization of the lasers and we show how three lasers can be stabilized using the fluorescence from a single atomic state. Laser spectroscopy of the $8p, 9p$, and $11p$–$15p$ states is then performed to determine the quantum defects of these states. Our measurement precision exceeds that of previous measurements of these defects by as much as a factor of 25. This work substantially extends our previous measurement of the $10p$ quantum defect, and we compare our measured defects with recent theoretical calculations for the *np* states across the range $8 \leq n \leq 15$. The agreement with theory is excellent.

1 Introduction

Spectroscopic measurements of the properties of Rydberg atoms provide powerful tests of our understanding of atomic physics [1–3]. High-resolution spectroscopy of Rydberg states usually requires the use of narrow bandwidth continuous wave lasers, where multiple lasers excite the Rydberg state through a series of intermediate states [4–8]. This technique, however, faces the challenge of keeping all lasers frequency-locked to their respective transitions.

Many different techniques exist to frequency stabilize lasers [9–17] but the simplest technique to implement for step-wise excitation is to use the atomic fluorescence intensity from each intermediate state to signal when each laser is at the correct optical frequency. However, the fluorescence from each state depends on the optical frequencies of at least two lasers, since at least two lasers interact with each intermediate state. This presents a difficulty for frequency stabilizing the lasers which we discuss and observe experimentally. We show that we can exploit the dependency of the fluorescence on the optical frequencies of multiple lasers to frequency lock three diode lasers using the fluorescence from a single atomic state, and then use a fourth laser to populate the Rydberg state.

We have excited a total of seven *np* Rydberg states in the range $8 \leq n \leq 15$ and report measurements of their atomic energies. These measurements are an extension of the work began in reference [8] where we measured the energy of the $10p$ atomic state. Combined with the measured $10p$ energy, the measurements presented here are consistently an order of magnitude more precise than previous experiments [18, 19] and cover the entire range $8 \leq n \leq 15$. In this way our measurements complement the precise measurements of atomic energies for *np* states with $n \leq 6$ [20] and $n \geq 15$ [21]. Our results are used to test the accuracy of recent calculations for the quantum defects of the lithium *np* series [22] and could be used as input for high accuracy measurements of electric fields using Rydberg atoms [6].

2 Experimental apparatus

An energy level diagram for ^{7}Li is shown in Fig. 1 and details of the lasers we use to excite the *np* Rydberg states are shown in Table 1. Three lasers: $L1$a, $L1$b, and $L2$ excite ^{7}Li to the $3S$, $F = 2$ state and a fourth laser, $L3$, excites from the $3S$ state to the *np* Rydberg state. Five separate $L3$

P. Oxley (✉) · P. Collins
Physics Department, College of the Holy Cross, 1 College St, Worcester, MA 01610, USA
e-mail: poxley@holycross.edu
Fax: +1-508-7933367

Published online: 08 August 2010

Table 1 Details of the diode lasers used to excite ^{7}Li to the *np* atomic state. Five different $L3$ lasers were used for the excitation step to the seven different Rydberg states. The beam sizes are approximate and for elliptical beams the first dimension is along a line in the direction of the lithium beam, and the second dimension is perpendicular to this line. The $10p$ state not listed in the table we have measured previously [8]

Laser	Excitation	Wavelength (nm)	Power (mW)	Beam shape/size
$L1$a	$2S, F = 2 \rightarrow 2P_{3/2}$	670.962	2	elliptical, 7 × 1 mm
$L1$b	$2S, F = 1 \rightarrow 2P_{3/2}$	670.961	2	elliptical, 7 × 1 mm
$L2$	$2P_{3/2}, \rightarrow 3S, F = 2$	812.869	4	elliptical, 5 × 1 mm
$L3$	$3S, F = 2 \rightarrow 8p$	687.460	9	elliptical, 3 × 2 mm
$L3$	$3S, F = 2 \rightarrow 9p$	670.594	4	circular, 3 mm dia.
$L3$	$3S, F = 2 \rightarrow 11p$	650.770	1.5	circular, 3 mm dia.
$L3$	$3S, F = 2 \rightarrow 12p$	644.619	22	circular, 2 mm dia.
$L3$	$3S, F = 2 \rightarrow 13p$	639.916	22	circular, 2 mm dia.
$L3$	$3S, F = 2 \rightarrow 14p$	636.236	6	elliptical, 4 × 2 mm
$L3$	$3S, F = 2 \rightarrow 15p$	633.300	6	elliptical, 4 × 2 mm

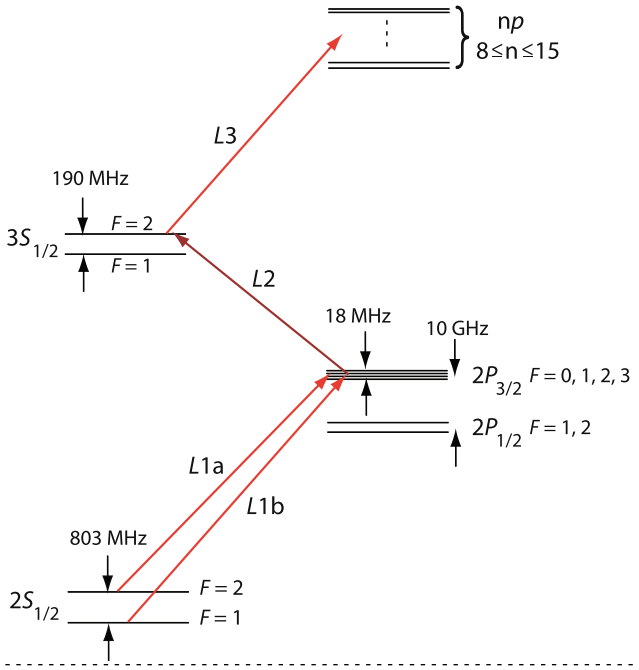

Fig. 1 Energy level diagram for ^{7}Li. Lasers $L1$a and $L1$b excite ^{7}Li to the $2P_{3/2}$ state from both ground state hyperfine levels. Laser $L2$ stimulates the $2P_{3/2} \rightarrow 3S, F = 2$ transition, and $L3$ subsequently excites to the *np* state. All four lasers can be simultaneously locked to their respective transitions

laser diodes were used to excite seven different *np* states. (The wavelengths of the $3S \rightarrow 12p, 13p$ transitions were close enough to be produced by one laser diode, as were the wavelengths of the $3S \rightarrow 14p, 15p$ transitions.) All lasers are grating stabilized diode lasers and the laser frequencies are controlled by applying a voltage to a piezo-electric transducer (PZT) mounted on the diffraction grating. The lasers' frequency spectra are monitored by a Fabry Perot interferometer and their wavelengths are recorded by a wavemeter (Advantest TQ8325). Laser $L1$a is polarized in the horizontal direction, parallel to the lithium beam, while $L1$b is polarized in the vertical direction. $L2$ is polarized at 60 degrees above the horizontal. $L3$, which intersects the atomic beam along a vertical axis, is polarized in a horizontal plane at 45 degrees to the atomic beam.

The principal benefit of exciting atoms from both ground state hyperfine levels by using both $L1$a and $L1$b is to increase the number of atoms excited to the $2P$ state, from where they can be subsequently excited to the Rydberg state. If only $L1$a were present, atoms which were initially in the $2S, F = 1$ state, or were optically pumped to this state, could not be excited to the Rydberg state. We find that with both $L1$a and $L1$b present we excite a factor of 5 more atoms to the $2P$ state than we do with $L1$a alone.

Figure 2 shows the lasers intersecting with a lithium beam produced by an oven in which natural lithium is heated to 470°C. The lithium atomic beam is collimated to a diameter of 4.5 mm at the location of the laser excitation where we estimate the lithium density to be 5×10^7 atoms/cm^3. The atomic beam has an angular divergence of 1.2° (full width). Close to the intersection of the lasers and the lithium beam are two large area (100 mm^2) photodiodes, PD_{2p} and PD_{3s}, used to detect $2P \rightarrow 2S$ and $3S \rightarrow 2P$ fluorescence, respectively. The photodiodes themselves are identical, but PD_{2p} is covered by an interference filter which transmits 60% of the incident light in a nominal 10 nm bandwidth centered on 670 nm, while PD_{3s} is covered by a similar filter centered on 810 nm.

As we will describe below, lasers $L1$a, $L1$b, and $L2$ can be frequency stabilized using only the signal from PD_{2p}. However, for the purpose of comparison we also include PD_{3s}, which can be used to lock $L2$. Including PD_{3s} increases the minimum possible distance between PD_{2p} and the lithium beam from 10 mm to 26 mm, which reduces by a factor of 7 the detected $2P \rightarrow 2S$ fluorescence. This factor

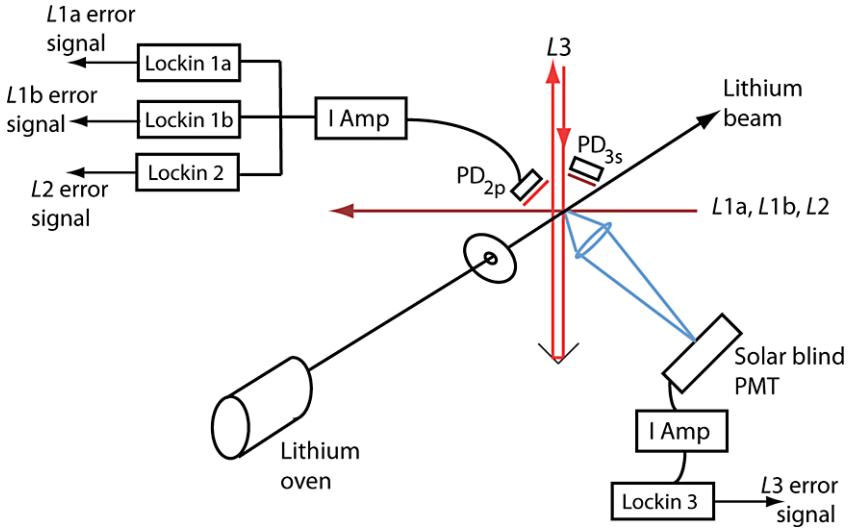

Fig. 2 Experimental apparatus used to excite ^{7}Li. A lithium beam produced by a home-built oven is intersected at *right angles* by four lasers. The apparatus shown is configured to frequency lock $L1$a, $L1$b, and $L2$ using the $2P$ fluorescence. To lock $L2$ using the $3S$ fluorescence Lock-in 2 would be connected to PD_{3s} via an additional current amplifier (I Amp)

of 7 is the gain we could therefore have made by not including PD_{3s} and by locking $L1$a, $L1$b, and $L2$ using only PD_{2p}. We note that the $2P_{3/2}$ state is composed of four unresolved hyperfine structure levels ($F = 0, 1, 2, 3$) separated by a total of 18 MHz. The exact frequency at which $L1$a and $L1$b will be stabilized is therefore expected to be somewhat closer to the higher F levels, which have the larger statistical weight.

A lens images fluorescence from the excitation region onto a photomultiplier tube (PMT) which detects the fluorescence emitted when the Rydberg state decays to the $2S$ ground state. This is the signal we use to indicate that $L3$ has successfully stimulated the $3S \rightarrow np$ transition. The standard approach of detecting fluorescence at the same wavelength as $L3$, i.e., from the $np \rightarrow 3S$ transition, is impractical for the $9p$ state. The fluorescence from this state has a wavelength of 671 nm and is swamped by the 671 nm fluorescence from the first excited state, which is approximately 10^4 times stronger. Fluorescence from the np states to the ground state, however, have wavelengths in the range 240 nm to 233 nm, which is very well separated from all other fluorescence wavelengths. We use a solar-blind PMT covered by a bandpass filter centered at 240 nm, which reduces the detected visible fluorescence to approximately 10% of the detected ultra-violet fluorescence. The frequency widths of the fluorescence detected by PD_{2p}, PD_{3s}, and the PMT are shown in Table 2.

For frequency stabilization, the frequency of each laser is dithered by applying a sinusoidal voltage to the PZT attached to the diffraction grating mounted in front of each laser diode. This results in a modulation of the fluorescence signals at the dither frequencies. The outputs of the photodiodes and the PMT which detect the fluorescence are fed to four lock-in amplifiers, one for each laser. Each lock-in amplifier measures the amount of fluorescence signal at one of the dither frequencies and provides an error signal used to correct the frequency of one of the lasers if it strays from resonance. Due to the relatively slow response of the PZTs the dither frequencies for the four lasers are less than 1 kHz. The time constants of the output filter on each lock-in amplifier are set to 100 ms, which is sufficiently short to allow for reliable locking of all lasers.

Table 2 Details of the frequency widths of the fluorescence detected during excitation to the np Rydberg state. The measured widths of the first two transitions are consistent with a combination of both Doppler and power broadening, while the final transition width is predominantly Doppler broadened. The Doppler width of the first two transitions is defined by the 1.2° angular divergence of the lithium beam. The width of the Rydberg transition is defined by the angle subtended by the volume of overlap of the four lasers which is ∼0.7° full width. The calculated Doppler broadenings for the laser transitions are: $L1$a and $L1$b, 55 MHz; $L2$, 45 MHz; and L3, 33 MHz

Fluorescence	Measured frequency width (MHz)	Broadening mechanism
$2P \rightarrow 2S$	90	Doppler + power
$3S \rightarrow 2P$	70	Doppler + power
$np \rightarrow 2S$	39	Doppler

3 Frequency stabilization of multiple lasers, theory

When an atom is excited by multiple laser fields, the populations of the atomic states depend on all of the lasers present. Since the fluorescence from these states is used to stabilize the frequency of each laser this coupling can lead to undesired effects. For example lasers $L1$a, $L1$b, and $L2$ all directly influence the population of the $2P_{3/2}$ state. Since fluorescence from this state is used to frequency stabilize $L1$a and $L1$b their stability can be adversely affected by the presence of laser $L2$.

Table 3 Possible frequency components present in the signal used to lock laser 1 (f_{LIA1}) and laser 2 (f_{LIA2})

f_{LIA1}	0	f_1	$2f_1$	$3f_1$	$\lvert f_2 - f_1\rvert$	$f_2 + f_1$	$2f_2 + f_1$	$\lvert 2f_2 - f_1\rvert$
f_{LIA2}	0	f_2	$2f_2$	$3f_2$	$\lvert f_2 - f_1\rvert$	$f_2 + f_1$	$2f_1 + f_2$	$\lvert 2f_1 - f_2\rvert$

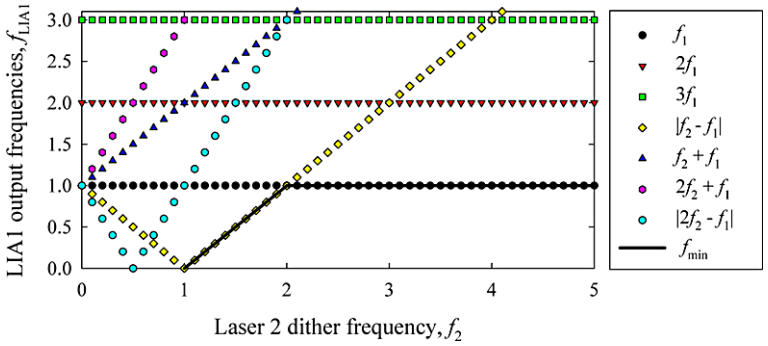

Fig. 3 Frequency components present in the output of LIA 1 as the dither frequency of laser 2 (f_2) is varied. Frequencies are scaled to the dither frequency of laser 1, i.e., $f_1 = 1$. A total of 7 frequency components are shown (equivalent to the 7 components in Table 3, excluding $f = 0$). The *solid line* shows the lowest frequency component present for all $f_2 > f_1$

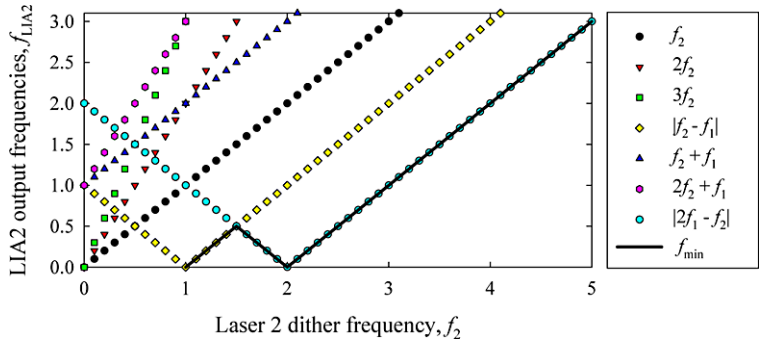

Fig. 4 Frequency components present in the output of LIA 2 as the dither frequency of laser 2 (f_2) is varied. Frequencies are scaled to the dither frequency of laser 1, i.e., $f_1 = 1$. A total of 7 frequency components are shown (equivalent to the 7 components in Table 3, excluding $f = 0$). The *solid line* shows the lowest frequency component present for all $f_2 > f_1$

To illustrate the potential difficulties which occur when locking multiple lasers we consider first a situation in which an atomic state is on resonance with two lasers dithered at frequencies f_1 and f_2, where $f_1 < f_2$.(These lasers could be any two of $L1$a, $L1$b, or $L2$ in our experiment and we will include the possibility of all three lasers below.) The fluorescence signal from the state can then contain frequency components f_1, f_2, $2f_1$ and $2f_2$. The first two frequencies occur when lasers 1 and 2 are near, but not on, resonance, and the second two occur when the lasers are on resonance. To stabilize the frequency of laser 1 a lock-in amplifier (LIA1) mixes the fluorescence signal with a reference signal at frequency f_1. The output of LIA1, which is fed back to laser 1 for frequency stabilization, can then contain the frequency components (f_{LIA1}) given in Table 3. If the same fluorescence signal is also being used to stabilize laser 2 it is fed to a second lock-in amplifier (LIA2). This lock-in amplifier mixes it with a reference frequency f_2 and its output can contain the frequency components f_{LIA2}, also shown in Table 3.

The zero (i.e., d.c.) frequency component in Table 3 is used to stabilize each laser when it strays from resonance. All other components are undesirable and must be removed to a satisfactory degree by the low pass filter on the lock-in amplifier output. We note that these components will, in general, have different amplitudes depending on how far off resonance is the laser and depending on the particular resonance line shape.

Figures 3 and 4 show graphically the frequency components f_{LIA1} and f_{LIA2} given in Table 3 (excluding the d.c. component), where we have set $f_1 = 1$. Emphasized in these figures is the minimum frequency component ($f_{\min}$) since this is the one which will be least attenuated by the lock-in amplifier output filter, and hence cause the greatest disturbance to efficient laser frequency stabilization. The zero frequency shown in Fig. 4 at $f_2 = 2$ (i.e., $f_2 = 2f_1$) represents a d.c. signal in the output of LIA2 that occurs when laser 1 is on resonance. This signal would not be attenuated at all by the output filter of LIA2 and would therefore erroneously change the frequency of laser 2, making efficient locking of this laser impossible. No such d.c. signal is present in laser 1 since $f_1 < f_2$.

Harmonics of the dither frequency are also in general present in the fluorescence signal (we have experimentally seen the second harmonic). When these are included the minimum frequency component in the LIA2 output is shown in Fig. 5, while the minimum component in the LIA1 output is unchanged from the solid line in Fig. 3. From Fig. 5 it can be seen that dither frequencies which are at integer

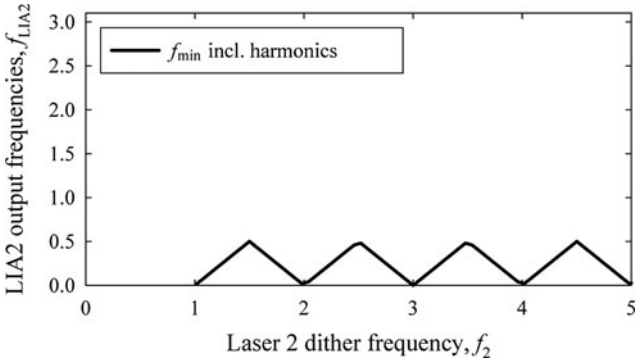

Fig. 5 The minimum frequency component present in the output of LIA 2 as the dither frequency of laser 2 is varied. This figure includes the effect of harmonics of the dither frequencies which may be present in the fluorescence signal

multiples of each other produce erroneous d.c. signals in the lock-in amplifier output.

Although an erroneous d.c. component is disastrous for frequency stabilization, low a.c. frequencies are also highly undesirable since they are not strongly attenuated by the lock-in output filter. From Fig. 5 we see that the optimum choice for dither frequencies is to have f_2 an odd half integer multiple of f_1. If this is not possible to arrange one must at least choose dither frequencies such that the minimum a.c. frequency component is much higher than the 3 dB cut-off frequency (f_c) of the output filter. This requirement, in terms of the lock-in output filter time constant, τ, is given by,

$$f_{\min} \gg f_c = \frac{1}{2\pi\tau}. \tag{1}$$

When locking three lasers the situation is more complicated but exactly the same ideas apply: the optimum choice of dither frequencies is that all dither frequencies are odd half integers of all other dither frequencies, and (1) must be satisfied.

4 Frequency stabilization of multiple lasers, experiment

The first step in exciting atoms to the Rydberg state is to efficiently populate the first excited state by stabilizing $L1$a to the $2S, F = 2 \rightarrow 2P_{3/2}$ transition and $L1$b to the $2S, F = 1 \rightarrow 2P_{3/2}$ transition. Stabilizing the $L1$a and $L1$b laser frequencies is performed using the $2P$ fluorescence, which contains components at the dither frequencies of the two lasers. In our experiment we choose to dither $L1$a at 553 Hz and $L1$b at 332 Hz. The ratio of these dither frequencies is 1.66, which is close to the optimum odd half integer multiple described in Sect. 3, and far from an integer multiple. Figure 6 shows the efficient and stable excitation to the $2P_{3/2}$ state with these dither frequencies, and also the

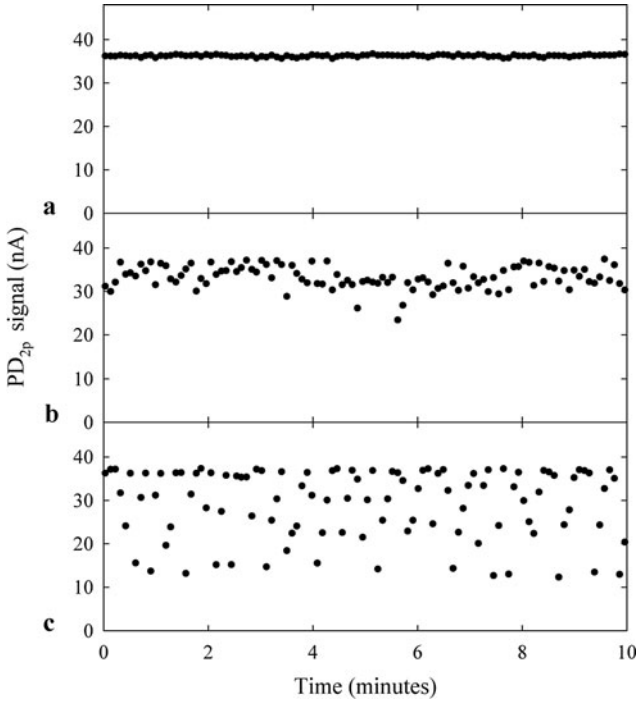

Fig. 6 Detected fluorescence from the $2P_{3/2}$ atomic state with both $L1$a and $L1$b locked. In (**a**) stable excitation of the $2P_{3/2}$ state is achieved with $L1$a and $L1$b dither frequencies of 553 Hz and 332 Hz (ratio 1.66). In (**b**) and (**c**) the $L1$a dither frequency is unchanged but the $L1$b dither frequency is 276.5 Hz (**b**) and 553 Hz (**c**). As expected from Fig. 4 stable excitation is not then possible

unstable excitation if we choose the dither frequencies to be equal, or one to be twice the other.

The next step in excitation to the Rydberg state is to lock laser $L2$ ($2P_{3/2} \rightarrow 3S, F = 2$) which can be done using the $3S$ fluorescence (the standard approach) or as we show here using the $2P$ fluorescence. Locking $L2$ using this second approach can be achieved since when $L2$ is on resonance, the $2P$ fluorescence is altered and we can exploit this change in fluorescence to produce a signal to lock $L2$. Figure 7 shows the changes in the $2P$ fluorescence, along with the $3S$ fluorescence, as the frequency of $L2$ is scanned across the $3S$ resonance with $L1$a and $L1$b locked. It is seen that when $L2$ is on resonance with the $2P_{3/2} \rightarrow 3S, F = 2$ transition there is a reduction in $2P$ fluorescence, while when it is on resonance with $2P_{3/2} \rightarrow 3S, F = 1$ there is an increase in $2P$ fluorescence. A simple explanation for a reduction in $2P$ fluorescence would be that if atoms spend a significant fraction of their time in a $3S$ state then they are not available to produce $2P$ fluorescence. This explanation clearly cannot account for *increases* in fluorescence and we believe it does not explain the reduction in fluorescence either. The explanation is lacking because it neglects coherences between the atomic states and quantum interference between different excitation paths to the $3S$ states.

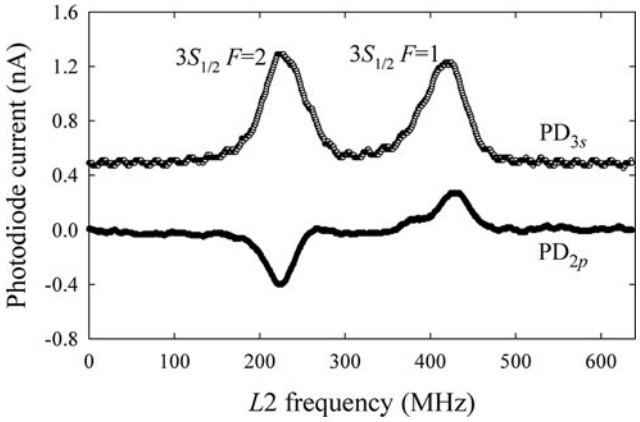

Fig. 7 $3S$ and $2P$ fluorescence as laser $L2$ frequency is scanned across the $3S$ states with $L1$a and $L1$b lasers locked. The two sets of data are offset for clarity. The fluorescence features at approximately 225 MHz are due to excitation of the $F = 2$ hyperfine component of the $3S$ state, while those at 415 MHz are due to excitation of the $F = 1$ component. We can use the dip in $2P$ fluorescence to lock $L2$

A full understanding of the effect $L2$ has on the $2P$ fluorescence requires modeling a five level atom ($2S\,F = 2$, $2S\,F = 1$, $2P_{3/2}$, $2P_{1/2}$, and $3S$) in which the two p levels have multiple nearly degenerate hyperfine structure components. Of these five levels the $2P_{1/2}$ state is populated only by spontaneous emission from the $3S$ state, and the other levels are directly influenced by the three laser fields present. Modeling a three non-degenerate level atom under the influence of two laser fields and spontaneous emission has been studied several decades ago [23, 24]. Since then there have been many more studies of the three possible laser excitation configurations ("V", "Λ", and "Ξ") for such a three level system, and variations on them to include a fourth level [25–28]. Such investigations have led to an understanding of the role played by atomic coherences and quantum interference between excitation amplitudes. These are responsible for a host of interesting effects, including coherent population trapping, electromagnetically induced transparency, and lasing without inversion. In our particular experiment lasers $L1$a, $L1$b, and $L2$ excite a combination of the Λ and Ξ configurations, which to our knowledge, has not yet been studied theoretically.

Given the lack of a theoretical treatment for our situation we performed three experimental tests to investigate the structure seen in the $2P$ fluorescence in Fig. 7. Firstly, we blocked laser $L1$b which transforms our $\Lambda + \Xi$ configuration into a Ξ configuration. In this case the peak in the $2P$ fluorescence shown in Fig. 7 was replaced by a dip, while the dip in fluorescence increased in width by approximately 60%. Similar results were found with laser $L1$a blocked and only $L1$b present. These results indicate that the structure seen in Fig. 7 is not a due simply to the Ξ configuration, but that the Λ part of the configuration is also important.

For the second test both $L1$ lasers and $L2$ were present, but excitation from the ground state was made to the $2P_{1/2}$ state, rather than the $2P_{3/2}$ state. Since the hyperfine splitting of the $2P_{1/2}$ state is 92 MHz, compared to 18 MHz for the $2P_{3/2}$ state, we can then resolve a single $2P_{1/2}$ hyperfine level. Excitation via the $2P_{1/2}$ state produced a fluorescence spectrum with a peak in place of the dip seen in Fig. 7. This suggests that quantum interference between $3S$ excitation pathways which proceed via different $2P_{3/2}$ hyperfine states is at least partly responsible for the structure seen in the $2P$ fluorescence of Fig. 7. Destructive quantum interference between the two excitation pathways $(2S, F = 2) \rightarrow (2P_{3/2}, F = 2) \rightarrow (3S, F = 1)$ and $(2S, F = 2) \rightarrow (2P_{3/2}, F = 1) \rightarrow (3S, F = 1)$ has previously been seen to occur when the $2S \rightarrow 2P$ and $2P \rightarrow 3S$ lasers have the same polarization [5]. This manifests itself as a very low probability for exciting the $3S, F = 1$ state and we have seen this effect ourselves by blocking $L1$b and rotating the polarization of $L2$ to be parallel to that of $L1$a.

Each hyperfine level is composed of $2F + 1$ nearly degenerate magnetic hyperfine states (these states are split by $\sim$1 MHz due to the Earth's magnetic field) and optical pumping effects could distribute the atomic populations unevenly between these magnetic states. This effect is sometimes used to populate a single magnetic state by applying circularly polarized radiation. In our experiment it would require a peculiar coincidence for a combination of three linearly polarized lasers, each polarized in a different direction, to produce such a concentration of population in a particular magnetic state. Whatever is the actual magnetic state population distribution we believe it is unlikely to play a large role in producing the structure seen in the $2P$ fluorescence. This assertion is supported by the fact that changing the polarization of $L2$ relative to $L1$a and $L1$b results in a largely unchanged $2P$ fluorescence spectrum.

The goal of the third test was to investigate the effect of coherences induced between the atomic states by the laser fields. In all previous experiments the laser intensities were such that the Rabi frequencies, Ω_{R}, for each transition were comparable to the line width of the lasers. This situation represents the boundary between when coherences are not significant (at lower Ω_{R}) and when they are significant [29]. In our experiment, the Rabi frequencies for $L1$a and $L1$b were 8 MHz, and $L2$ was 16 MHz, while the laser line widths were measured to be 6 MHz for $L1$a and $L1$b, and 10 MHz for $L2$. In the third test, excitation to the $3S$ states proceeded with $L1$a, $L1$b, and $L2$ all present and with both $L1$ lasers again exciting the $2P_{3/2}$ state, but with the laser intensities reduced by a factor of 6.5. This reduces Ω_{R} by a factor of 2.5, which should significantly reduce the role played by atomic coherences. The reduction in intensity was achieved by increasing the laser beam sizes, which also had the effect of allowing them to interact with more atoms in the

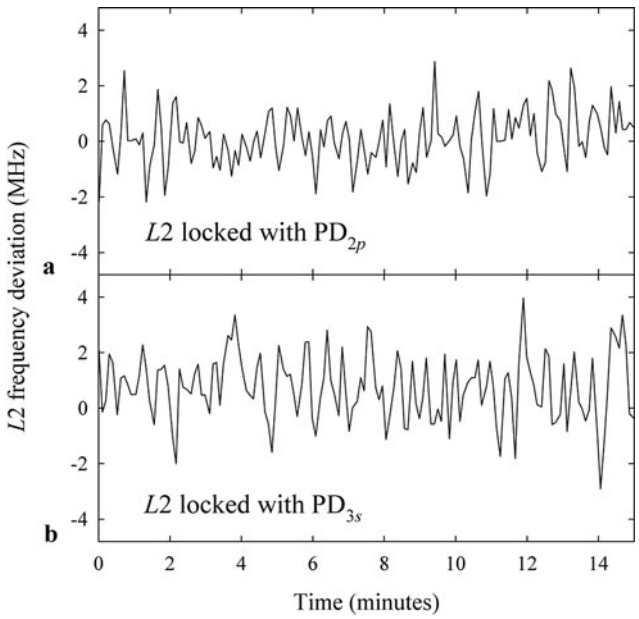

Fig. 8 Frequency stability of $L2$ when locked using (**a**) the $2P$ fluorescence and (**b**) the $3S$ fluorescence. The locking stability is seen to be similar in the two cases and sufficient to keep $L2$ locked close to the center of the $2P_{3/2} \rightarrow 3S_{1/2}$ transition of width 70 MHz (Table 2)

atomic beam. As a consequence, the level of fluorescence detected with the lower intensity lasers was not reduced. In this lower intensity test the $2P$ fluorescence structure seen in Fig. 7 disappeared entirely, suggesting that coherences between the atomic states play a key role in the structure of the $2P$ fluorescence.

We suggest then, that the $2P$ fluorescence structure seen in Fig. 7 relies on atomic state coherences and quantum interference between different hyperfine excitation pathways in the $\Lambda + \Xi$ configuration. We note that in all the different combinations of tests we have tried, except the low intensity test with $L1$a, $L1$b, and $L2$ present, features in the $2P$ fluorescence spectrum exist which can be used to lock $L2$.

To stabilize the frequency of $L2$ we use the dip in $2P$ fluorescence when $L2$ is on resonance with the $3S$, $F = 2$ hyperfine component, and thus stabilize $L1$a, $L1$b, and $L2$ using only the $2P$ fluorescence. $L2$ is dithered at $f_3 = 871$ Hz (a factor of 1.58 higher than $L1$ dither frequency, and a factor of 2.62 higher than the $L1$b dither frequency). The frequency stability of $L2$ is shown in Fig. 8(a). In Fig. 8(b) the $L2$ frequency stability is shown when $L2$ is locked using the $3S$ fluorescence (the standard approach). It is seen that the laser stability is equally as good when using our new method of locking $L2$, compared to the standard method. We note that whichever fluorescence is used to lock $L2$ the fluorescence will contain frequency components at all dither frequencies. Using the standard method to lock $L2$ does not avoid this problem, and an appropriate choice of dither frequencies (e.g., odd half integers) must still be made.

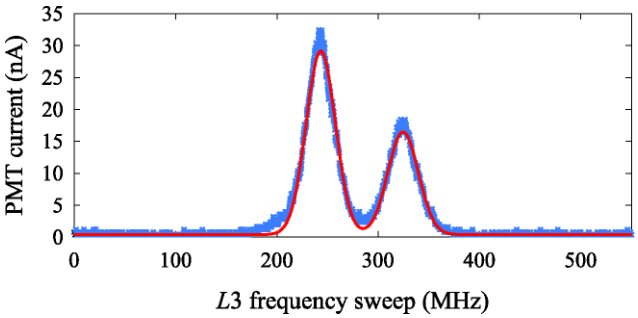

Fig. 9 $9p \rightarrow 2S$ fluorescence as laser $L3$ frequency is swept across the $3S$ $F = 2 \rightarrow 9p$ resonance. The *blue crosses* are the experimental data and the *red line* is a two-Gaussian fit to the data. The two $9p$ fine structure components are well resolved with good signal to noise

5 Spectroscopy of Rydberg states

With $L1$a, $L1$b, and $L2$ all locked using the $2P$ fluorescence, laser $L3$ is used to excite the Rydberg states. Figure 9 shows fluorescence from the $9p$ Rydberg state to the ground state as the frequency of $L3$ is swept across the $3S_{1/2}$ $F = 2 \rightarrow 9p$ transition. The frequency calibration for this data is made using a Fabry–Pérot interferometer to monitor $L3$ frequency while the sweep is in progress. In Fig. 9 the two peaks correspond to the two fine structure components of the $9p$ state. Similar spectra are recorded for the other $3S_{1/2}$ $F = 2 \rightarrow np$ transitions in the range $8 \leq n \leq 15$. Due to the n^{-3} scaling of the fine structure interval we find that above $n = 11$ the two fine structure components are not well resolved. We can lock the frequency of $L3$ to either of the fine structure components for $n \leq 11$, or to the peak of the unresolved components for the higher n states. In this way we create a continuous source of Rydberg atoms.

The energy of the Rydberg states above the $2S$ ground state is straightforwardly inferred from a measurement of the wavelength of $L3$ required to excite each Rydberg state. This wavelength is reported by our wavemeter, the accuracy of which is confirmed by measuring the wavelengths of the lithium D_2 lines, which are very accurately known [30] and the wavelength of the 633 nm helium–neon line. The wavemeter reports the wavelengths of the $3S_{1/2}$, $F = 2 \rightarrow np$ center of gravities, which are listed in Table 1. Each wavelength measurement has an uncertainty of ± 0.001 nm, which comes from the last reported wavemeter digit. Locking $L3$ is not necessary for measuring this wavelength since the $L3$ frequency drift over the duration of the measurement is negligible compared to the wavemeter uncertainty.

In addition to the wavemeter uncertainty, uncertainties in the $3S$, $F = 2 \rightarrow np$ wavelength due to three other effects were considered. These are summarized in Table 4 for the $15p$ state, for which the uncertainties are the greatest. Foremost amongst these uncertainties is a Doppler shift in the $3S$, $F = 2 \rightarrow 15p$ wavelength due to non-perpendicular intersection of the laser and atomic beams. By using a retro-

Table 4 Uncertainties in MHz for the energy of the $15p$ state measured in this paper. The values for the Doppler shift assume a $\pm 2°$ uncertainty in the perpendicular alignment of the laser and atomic beams. The values for Zeeman and Stark shifts assume fields of 0.5 G and 0.1 V/cm. The total uncertainty is 745 MHz, or 0.025 cm^{-1}

Source of uncertainty	Uncertainty (MHz)
Wavemeter accuracy	740
Doppler shift	95
Zeeman shift	<1
Stark shift	<1

Table 5 Measured energies and quantum defects of the $8p$, $9p$, and $11p$–$15p$ states

	E_{np} (cm^{-1})	δ_{np}
$n = 8$	41752.397 (21)	0.04683 (5)
$n = 9$	42118.249 (22)	0.04692 (7)
$n = 11$	42572.509 (23)	0.04701 (13)
$n = 12$	42719.136 (24)	0.04711 (19)
$n = 13$	42833.148 (24)	0.04709 (24)
$n = 14$	42923.535 (25)	0.04708 (31)
$n = 15$	42996.401 (25)	0.04707 (38)

reflector to reflect back laser $L3$ once it has passed through the lithium beam, we make a conservative estimate that the laser and atomic beams are perpendicular to better than 2°. This corresponds to a 95 MHz Doppler shift. Shifts in the Rydberg state energy due to the Earth's magnetic field and due to stray electric fields were also considered. In the Earth's magnetic field of 0.5 G, and in a stray electric field of 0.1 V/cm the $15p$ state is shifted by less than 1 MHz.

To infer the energy of the np Rydberg state (E_{np}) from the wavelength of the $3S$, $F = 2 \rightarrow np$ transition we use the known values of the energy of the center of gravity of the $3S$ state (27,206.094082 (6) cm^{-1} [31]) and the $3S$ hyperfine splitting (0.00621166 (74) cm^{-1} [32]). Using these we calculate the energy of the Rydberg states above the ground state and our results are shown in Table 5. The quantum defects of the np states, δ_{np}, are given by

$$\delta_{np} = n - \sqrt{109728.73/(E_I - E_{np})}, \quad (2)$$

where E_I is the ^{7}Li ionization potential (43,487.15940 (18) cm^{-1} [7]). The defects are also included in Table 5.

Of the measurements shown in Table 5, France has previously measured the energies of all but the $11p$ state [18] and Ballard has measured all but the $15p$ state [19]. The $15p$ state has been measured by Anwar-ul-Haq [21]. In Fig. 10 the quantum defects shown in Table 5 are compared with those inferred from the most precise measurements of [18, 19, 21] and recent theoretical calculations of Chen [22]. It is

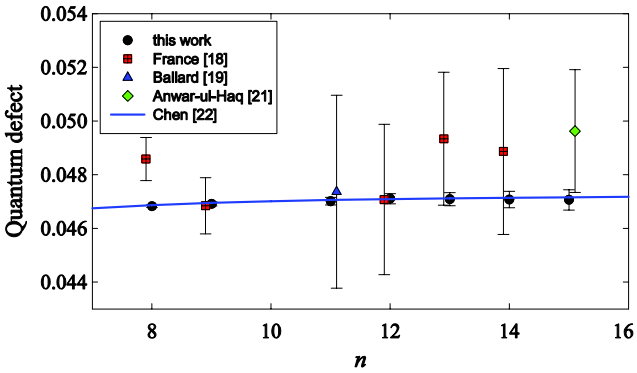

Fig. 10 Comparison between the quantum defect measurements made in this work and in previous experiments. Also displayed is the theoretical prediction of Chen [22], which is shown in more detail in Fig. 11

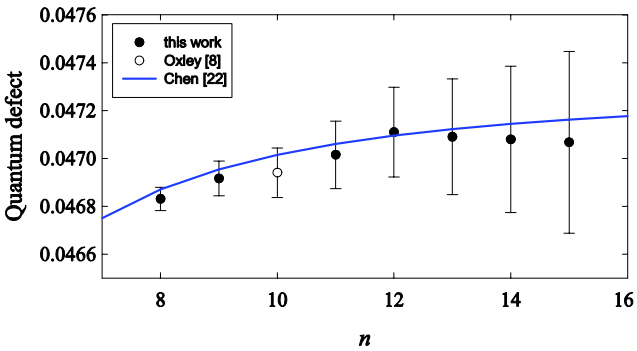

Fig. 11 Comparison between the quantum defect measurements of this work and the QDF predictions of Chen [22]. The hollow point at $n = 10$ indicates the measurement made previously by the current authors [8]

seen from the figure that the measurements reported in our work are significantly more precise than those previously reported. They range from a factor of 25 more precise for $n = 11$ to a factor of 6 more precise for $n = 15$.

The theoretical calculations of Chen use a combination of experimental data for the lithium np energy levels with $n \leq 7$ [33] and R-matrix calculations to determine the quantum defect function (QDF) for the np series. In Fig. 11 we show a comparison of our results and the QDF on a scale ten times smaller than that of Fig. 10. For completeness the defect of the $10p$ state from our previous measurement [8] is also included in Fig. 11. From both Figs. 10 and 11 it is clear that our defect measurements agree very well with the theoretical predictions.

6 Conclusions

We have described an experimental apparatus used to excite lithium atoms to a Rydberg state using a total of four diode lasers. The atomic fluorescence is seen to be dependent on the optical frequencies of multiple lasers, which

could potentially lead to difficulties when frequency stabilizing them to their respective atomic transitions. We have reviewed these difficulties and use this dependence to advantage to allow frequency stabilization of three of the lasers using only a single fluorescence signal. By frequency stabilizing all four lasers we can produce a continuous beam of Rydberg atoms, which will be used in future collision experiments in our laboratory. We have excited seven np Rydberg states in the range $8 \leq n \leq 15$. These low Rydberg states are too tightly bound to be easily detected by selective field ionization and one must use an alternative detection technique, such as detecting the ultra-violet fluorescence from the Rydberg state to the ground state, as described here. We have made significant improvements in the measurement precision of the energies of the np states excited, and the quantum defects inferred from our energy measurements are found to be in excellent agreement with theoretical calculations.

References

1. T.F. Gallagher, *Rydberg Atoms* (Cambridge University Press, Cambridge, 1994)
2. E. Arimondo, M. Inguscio, P. Violino, Rev. Mod. Phys. **49**, 31 (1977)
3. M.L. Zimmerman, M.G. Littman, M.M. Kash, D. Kleppner, Phys. Rev. A **20**, 2251 (1979)
4. R. Hergenroder, D. Veza, K. Niemax, Spectrochim. Acta **48B**, 589 (1993)
5. C.-H. Iu, G.D. Stevens, H. Metcalf, Appl. Optics **34**, 2640 (1995)
6. G.D. Stevens, C.-H. Iu, T. Bergeman, H.J. Metcalf, I. Seipp, K.T. Taylor, D. Delande, Phys. Rev. A **53**, 1349 (1996)
7. B.A. Bushaw, W. Nörtershäuser, G.W.F. Drake, H.-J. Kluge, Phys. Rev. A **75**, 052503 (2007)
8. P. Oxley, P. Collins, Phys. Rev. A **81**, 024501 (2010)
9. R.W.P. Drever, J.L. Hall, F.V. Kowalski, J. Hough, G.M. Ford, A.J. Munley, H. Ward, Appl. Phys. B **31**, 97 (1983)
10. W. Jitschin, Appl. Phys. B **33**, 7 (1984)
11. H.R. Telle, Spectrochim. Acta Rev. **15**, 301 (1993)
12. G. Bianchini, P. Cancio, F. Minardi, F.S. Pavone, F. Perrone, M. Prevedelli, M. Inguscio, Appl. Phys. B **66**, 407 (1998)
13. K.L. Corwin, Z.-T. Lu, C.F. Hand, R.J. Epstein, C.E. Wieman, Appl. Optics **37**, 3295 (1998)
14. C.P. Pearman, C.S. Adams, S.G. Cox, P.F. Griffin, D.A. Smith, I.G. Hughes, J. Phys. B **35**, 5141 (2002)
15. G. Ritt, G. Cennini, C. Geckeler, M. Weitz, Appl. Phys. B **79**, 363 (2004)
16. E.D. Van Ooijen, G. Katgert, P. Van der Straten, Appl. Phys. B **79**, 57 (2004)
17. J.A. Kerckhoff, C.D. Bruzewicz, R. Uhl, P.K. Majumder, Rev. Sci. Instrum. **76**, 093108 (2005)
18. R.W. France, Proc. R. Soc. Lond., Ser. A **129**, 354 (1930)
19. M.K. Ballard, R.A. Bernheim, P. Bicchi, Can. J. Phys. **79**, 991 (2001)
20. L.J. Radziemski, R. Engleman Jr., J.W. Brault, Phys. Rev. A **52**, 4462 (1995)
21. M. Anwar-ul-Haq, S. Mahmood, M. Riaz, R. Ali, M.A. Baig, J. Phys. B **38**, S77 (2005)
22. C. Chen, Commun. Theor. Phys. **50**, 733 (2008)
23. R.M. Whitley, C.R. Stroud, Phys. Rev. A **14**, 1498 (1976)
24. C. Cohen-Tannoudji, S. Reynaud, J. Phys. B **10**, 2311 (1977)
25. C. Wei, D. Suter, A.S.M. Windsor, N.B. Manson, Phys. Rev. A **58**, 2310 (1998)
26. C. Mavroyannis, Appl. Phys. B **73**, 39 (2001)
27. K. Kapale, M.O. Scully, S.-Y. Zhu, M. Suhail Zubairy, Phys. Rev. A **76**, 023804 (2003)
28. B.-Q. Ou, L.-M. Liang, C.-Z. Li, J. Phys. B **42**, 205503 (2009)
29. H.R. Gray, R.M. Whitley, C.R. Stroud, Opt. Lett. **3**, 218 (1978)
30. C.J. Sansonetti, B. Richou, R.E. Engleman, Phys. Rev. A **52**, 2682 (1995)
31. R. Sánchez, R. Sánchez, M. Žáková, Z. Andjelkovic, B.A. Bushaw, K. Dasgupta, G. Ewald, C. Geppert, H.-J. Kluge, J. Krämer, M. Nothhelfer, D. Tiedemann, D.F.A. Winters, W. Nörtershäuser, New J. Phys. **11**, 073016 (2009)
32. B.A. Bushaw, W. Nortershauser, G. Ewald, A. Dax, G.W.F. Drake, Phys. Rev. Lett. **91**, 043004 (2003)
33. I. Johansson, Ark. Fys. **15**, 169 (1959)